Eur. Phys. J. Spec. Top. (2026) 235:8711–8722
https://doi.org/10.1140/epjs/s11734-026-02597-0

THE EUROPEAN PHYSICAL JOURNAL SPECIAL TOPICS

Regular Article

Multistability, chaos, and transient dynamics in an avian influenza mathematical model

Ana Luiza de Moraes[1,a], Fátima E. Cruziniani[2,3], Enrique C. Gabrick[1], Antonio M. Batista[2,3], Iberê L. Caldas[1], and Jürgen Kurths[4,5,6]

[1] Institute of Physics, University of São Paulo, 05508-090, São Paulo, Brazil
[2] Graduate Program in Science, State University of Ponta Grossa, 84030-900 Ponta Grossa, PR, Brazil
[3] Department of Mathematics and Statistics, State University of Ponta Grossa, 84030-900 Ponta Grossa, PR, Brazil
[4] Potsdam Institute for Climate Impact Research, Telegrafenberg A31, 14473 Potsdam, Germany
[5] Department of Physics, Humboldt University Berlin, Newtonstraße 15, 12489 Berlin, Germany
[6] Research Institute of Intelligent Complex Systems, Fudan University, 220 Handan Rd, 200437 Yangpu District, Shanghai, China

Received 17 March 2026 / Accepted 19 August 2026 / Published online 26 August 2026
© The Author(s) 2026

Abstract Influenza, commonly known as the flu, is a highly contagious respiratory infection that causes symptoms, such as cough, aches, and malaise in infected individuals. One important form of influenza A infection is avian influenza, caused by the H5N1 virus, which has been a concern since the late twentieth century due to its high mortality rate. Monitoring and controlling avian influenza is of great importance for public health issues due to its ability to infect other mammals and its potential risk for spillover to humans. Mathematical models capable of describing the dynamics of avian influenza have been proposed to explore the spread of the disease and adapt control measures to contain it. In this work, we analyze the dynamical behavior of an avian influenza model consisting of two coupled SI (susceptible-infected) models, one describing the bird population and the other the human population. Using the bird mortality rate as the control parameter and hysteresis-type bifurcation diagrams, we identify bistability over a wide parameter range. As this parameter increases, we observe a significant range of hyperchaos. Furthermore, we uncover and quantify transient chaos and boundary crises for a given set of parameter values. These findings contribute to a more detailed understanding of the non-linear dynamics that may arise in mathematical models of avian influenza transmission.

1 Introduction

Influenza is an acute infection of the respiratory system. It is caused by the influenza virus and is highly contagious. The disease is classified into A, B, and C types [1]. Avian influenza is type A [2] and is classified according to the pathogenicity index, which can be High Pathogenicity Avian Influenza (HPAI) or Low Pathogenicity Avian Influenza (LPAI). HPAI is caused by the H5N1 virus [3]. The first outbreak in chickens was reported in Scotland in 1965 [4]. In 1996, the first isolation of the H5N1 virus was made in geese in southern China. In 1997, an outbreak occurred in Hong Kong, leading to 18 reported cases of human infection, six of which were fatal [5, 6]. Since 2003, new cases have been detected in Asia and later outside the Asian region, reaching Europe, Africa, and the Americas. The H5N1 subtype is predominant and this means that the virus has the potential to infect humans, horses, pigs, birds, and other mammals [7]. Since 2024, HPAI H5N1 outbreaks have occurred in dairy cattle in several states of the United States, raising a significant global health concern, highlighting the ability of the virus to adapt to new mammalian hosts [8]. Therefore, HPAI poses a greater risk to these populations and consequently represents a significant public health concern, underscoring the urgency of studies to understand its propagation dynamics.

The 1918 Spanish Flu, one of the deadliest pandemics in history with an estimated 40–100 million deaths [9], was caused by the H1N1 virus. In 2005, a phylogenetic analysis was carried out and it was identified that the origin of the virus was avian and not swine, contradicting the prevailing idea at the time. The influenza virus has

[a] e-mail: a_moraes@usp.br (corresponding author)

a segmented RNA genome [10], and, therefore, has a high capacity to undergo mutations, allowing it to adapt to humans without the need for animal intermediaries, which explains its high pathogenicity and lethality.

Avian influenza spreads readily among domestic and wild birds of different species, facilitating intercontinental spread and hindering control efforts. Transmission between birds might occur through aerosols and respiratory secretions, feces, or contaminated body fluids, through direct contact (proximity to the host) or indirect contact (contaminated water or fomites) with the virus [3]. Transmission from birds to humans can occur through contact with infected birds, contaminated environments, or even fertilizers that contain the feces of these birds [11].

Mathematical models are a powerful tool in terms of epidemic modeling, allowing simulation of mitigation strategies and forecasting [12]. In terms of avian flu, Iwami et al. introduced an epidemic model that enables a precise description of the dynamics of avian influenza [6]. They proposed an interaction between birds and humans described by an SI-SIR model. Their findings suggest that there is an imminent possibility of two outbreaks of avian influenza if no control measures are provided. Motivated by a real-time series of avian flu and climate data, Tuncer and Martcheva [13] incorporated a seasonality forcing term into the model for direct transmission of H5N1 to bird populations. Their results support the notion that seasonality in bird susceptibility can be an explanation for the periodicity observed in H5N1 cases.

Time series and theoretical studies have shown that avian influenza exhibits pronounced seasonal trends. Taking into account different strains of influenza A, Martcheva [14] argued that certain models can exhibit complex dynamical behavior, the main characteristic of which are oscillations occurring under a constant value of the infection transmission rate. For a time window from 1997 to 2006, Park and Glass [15] studied outbreaks throughout the Western and Southwestern Asia region. They found a strong seasonality in the transmission of diseases from bird to bird, concluding that outbreaks occur mainly in winter. Li et al. [16] showed that the cases in wild birds in Northwest Asia of China correspond to the migratory movements of birds, with outbreaks occurring predominantly when birds return and gather in breeding areas during winter. Tuncer and Martcheva [13] analyzed avian influenza outbreaks in regions of Egypt and Indonesia, two countries that recorded a large number of outbreaks in humans and birds, in 2005 and 2006, based on data provided by Murray and Morse [17]. Their research demonstrated a link between low temperatures and high intensity in transmissions in Egypt. However, in Indonesia, the temperature remained almost constant throughout the year and, therefore, it was not possible to reach the same conclusion. Cruziniani et al. [18] investigated a non-autonomous epidemic model for avian influenza in humans, considering seasonality. They observed that initial conditions and control parameters play a key role in the number of outbreaks. In addition, the number of outbreaks increases when considering the growth in the rate of contact between infected people, no matter how small, resulting in a higher number of outbreaks during the winter. These findings justify modeling the transmission of avian influenza among birds at a seasonal rate, capturing the migratory and climatic effects [19].

Viral mutation factors are the main concern regarding the emergence of a pandemic caused by the H5N1 virus. Mutations are characterized by randomness and unpredictability. Mathematical models based on real data have proven to be effective in making predictions and improving epidemic control strategies. However, when the parameters are set in chaotic regions, the predictability is drastically affected. The chaotic dynamics present in infectious diseases is observed in both real-time series [20, 21] and synthetic data produced by compartmental models within ranges of parameters with biological meaning [22].

The non-linear interactions present in epidemiological compartmental models can generate rich dynamical solutions, including chaos in multi-strain epidemic systems [23, 24] and chaos induced by seasonal forcing [25, 26]. In seasonally forced models, increasing the intensity of the forcing leads to period-doubling cascades and chaotic dynamics for given parametric settings [27, 28], providing an explanation for the recurrent oscillations observed in childhood infectious diseases [29] and dengue epidemics [30]. Beyond chaos, epidemiological systems can exhibit multistability, where multiple attractors coexist for the same parameter set [31]. These attractors can emerge or disappear through bifurcations and crisis events, giving rise to abrupt dynamical transitions and transient chaotic behavior [32, 33]. Together, these studies demonstrate that compartmental epidemic models show remarkable properties of interest in non-linear phenomena.

However, despite the extensive literature on chaos and multistability in epidemiological systems, most studies have focused on single-population models or generic epidemic frameworks. Comparatively less attention has been devoted to seasonally forced models coupling distinct host populations, particularly bird-human transmission systems, which is highly relevant to avian influenza scenarios. In the specific model proposed by Tuncer and Martcheva [13], previous analyses reported bifurcation structures and chaotic dynamics, but several important non-linear phenomena remained unexplored, including attractor coexistence, basin organization, crisis-induced transitions, transient chaos, and hyperchaos.

In this work, we extend the analysis of Tuncer and Martcheva's model [13] by investigating additional non-linear dynamical phenomena. First, we revisit the previously reported chaotic dynamics through bifurcation diagrams and Lyapunov exponent calculations. Then, we demonstrate that the model exhibits multiple bistable regimes, including both periodic-periodic and chaotic-periodic attractor coexistence, identified through hysteresis-type bifurcation diagrams and Lyapunov spectra. Furthermore, we characterize the corresponding basins of attraction and show that their boundaries remain smooth over the investigated parameter ranges. We also uncover a boundary crisis

leading to long-lived transient chaos and quantify its scaling properties. Finally, we identify hyperchaotic regimes characterized by two positive Lyapunov exponents. Therefore, while chaos and multistability have been previously reported in epidemic models [34–38], the principal contribution of the present work is to demonstrate the coexistence of attractors, crisis-induced transitions, transient chaos, and hyperchaos, thus providing a broader characterization of the non-linear dynamics exhibited by the bird-human disease transmission model.

This work is structured as follows: In Sect. 2, we revise a mathematical model by computing the stability, the basic reproduction number, and the bifurcation diagram. In Sect. 3, we show the existence of bistable solutions for a given parameter range. In Sect. 4, we study transient chaos and the existence of boundary crisis. Thereafter, we explore the existence of hyperchaotic solutions in Sect. 5. Finally, we draw our conclusions and summarize the main findings in Sect. 6.

2 The avian influenza mathematical model

To investigate the non-linear phenomena discussed above, we consider the seasonally forced avian influenza model proposed by Tuncer and Martcheva [13]. This model captures the transmission dynamics between bird (susceptible (S_b) and infected (I_b)) and human (susceptible (S_h) and infected (I_h)) populations and provides a grounded framework for exploring bifurcations, chaos, and multistability. The model is governed by the following set of equations:

$$\begin{aligned}
\frac{dS_b}{dt} &= \nu - \alpha(t) S_b I_b - \rho S_b, \\
\frac{dI_b}{dt} &= \alpha(t) S_b I_b - (\rho + \chi) I_b, \\
\frac{dS_h}{dt} &= \lambda - \beta S_h I_b - \mu S_h, \\
\frac{dI_h}{dt} &= \beta S_h I_b - (\mu + \delta) I_h,
\end{aligned} \tag{1}$$

subject to positive initial conditions, i.e., $S_b(0)$, $I_b(0)$, $S_h(0)$, $I_h(0) \geq 0$.

In Eq. (1), ν is the birth rate of birds, ρ is the natural death rate of birds, χ is the mortality rate induced by HPAI for birds, and α is the transmission rate of avian influenza among birds. The parameter λ is the birth rate of humans, μ is the natural death rate of humans, δ is the death rate of humans due to avian influenza, and β is the transmission coefficient of avian influenza from birds to humans. Humans are infected through spillover transmission from infected birds, which establishes transmission between species. The model and transmission mechanism are illustrated in Fig. 1.

The parameter α is an explicit function of the independent variable t, known as a seasonal contact rate [39], and is given by

$$\alpha(t) = \kappa_1 \sin\left[\frac{2\pi}{365}(t + \omega)\right] + \kappa_2, \tag{2}$$

where the parameters κ_1, κ_2, and ω correspond to the amplitude, vertical displacement, and phase shift, respectively, and are all obtained through the fitting procedure described in [13]. Due to this time-dependent forcing, the model is non-autonomous. For physical meanings, $\kappa_1 \leq \kappa_2$ and $\alpha \geq 0 \ \forall \ t$, where $t \geq 0$. For numerical purposes, as computing the Lyapunov exponents, we transform the system from non-autonomous to autonomous by making the transformation $\omega = t$, where $\dot{\omega} = 1$. This transformation gives an autonomous system, but adds one dimension.

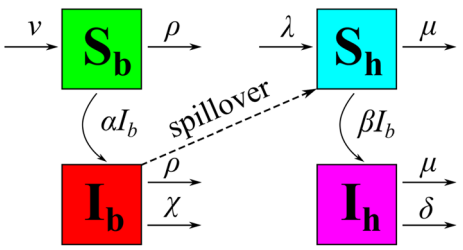


Fig. 1 Flowchart of the avian influenza model

The equilibrium states of this model can be determined by solving the following equations:

$$0 \equiv \nu - \alpha(t) S_b I_b - \rho S_b, \tag{3}$$

$$0 \equiv \alpha(t) S_b I_b - (\rho + \chi) I_b, \tag{4}$$

$$0 \equiv \lambda - \beta S_h I_b - \mu S_h, \tag{5}$$

$$0 \equiv \beta S_h I_b - (\mu + \delta) I_h, \tag{6}$$

where the disease-free equilibrium (DFE) is $\mathcal{E}_0 = (\hat{S}_b, \hat{I}_b, \hat{S}_h, \hat{I}_h) = (\nu/\rho, 0, \lambda/\mu, 0)$. Another important equilibrium solution is the endemic equilibrium, which is given by $\mathcal{E}_1 = (S_b^*, I_b^*, S_h^*, I_h^*)$, each of them being

$$S_b^* = \frac{\rho + \chi}{\alpha(t)}, \tag{7}$$

$$I_b^* = \frac{\nu}{\rho + \chi} - \frac{\rho}{\alpha(t)}, \tag{8}$$

$$S_h^* = \frac{\lambda}{\beta I_b^* + \mu}, \tag{9}$$

$$I_h^* = \frac{\beta S_h^* I_b^*}{\mu + \delta}. \tag{10}$$

For the autonomous case, i.e. $\alpha(t) = \text{const.}$, the basic reproduction number is $\mathcal{R}_0 = \dfrac{\alpha\nu}{\rho(\rho + \chi)}$. In this case, when $\mathcal{R}_0 < 1$, all solutions asymptotically reach $\mathcal{E}_0$, otherwise all solutions approach the state $\mathcal{E}_1$ when $\mathcal{R}_0 > 1$. For the first case, the endemic point is unstable while $\mathcal{E}_0$ is stable. On the other hand, when $\mathcal{R}_0 > 1$, the equilibrium points exchange stability via a transcritical bifurcation that occurs at the bifurcation point $\mathcal{R}_0 = 1$. Furthermore, it is possible to attest that for $\beta \neq 0$, infected humans are a direct consequence of infected birds [13].

2.1 $\mathcal{R}_0$ for non-autonomous case

Unlike the previous case, the non-autonomous formulation requires a deeper analysis and calculating $\mathcal{R}_0$ is not straightforward. To determine the local behavior of the solutions around each critical point $(\hat{S}_b, \hat{I}_b)$ of a non-linear system, we relate a function $f(x) = dx/dt$ to a corresponding linear system through the system of equations

$$\frac{d}{dt}\begin{pmatrix} s(t) \\ i(t) \end{pmatrix} = \begin{pmatrix} F_{S_b}(\hat{S}_b, \hat{I}_b) & F_{I_b}(\hat{S}_b, \hat{I}_b) \\ G_{S_b I_b}(\hat{S}_b, \hat{I}_b) & G_{I_b}(\hat{S}_b, \hat{I}_b) \end{pmatrix} \begin{pmatrix} s(t) \\ i(t) \end{pmatrix}, \tag{11}$$

which are $s(t) = (S_b(t) - \hat{S}_b)$ and $i(t) = (I_b(t) - \hat{I}_b)$, and $F(\hat{S}_b, \hat{I}_b)$ and $G(\hat{S}_b, \hat{I}_b)$ are functions that are twice differentiable.

For the equilibrium $\mathcal{E}_0 = (\nu/\rho, 0)$, the solutions become $S_b(t) = s(t) + \nu/\rho$ and $I_b(t) = i(t) + 0 = i(t)$. Then, Eq. (11) becomes

$$\frac{d}{dt}\begin{pmatrix} s(t) \\ i(t) \end{pmatrix} = \begin{pmatrix} -\rho s(t) - \alpha(t)\dfrac{\nu}{\rho} i(t) \\ \alpha(t)\dfrac{\nu}{\rho} i(t) - (\rho + \chi) i(t) \end{pmatrix}. \tag{12}$$

The solution for $i(t)$ takes the form

$$i(t) = i(0) \exp\left[\int_0^t \left(\alpha(s)\frac{\nu}{\rho} - (\rho + \chi)\right) ds\right]. \tag{13}$$

Before proceeding, we consider the long-term average of a function $\langle f \rangle$ [39, 40], defined by

$$\langle f \rangle = \lim_{t \to \infty} \frac{1}{t} \int_0^t f(s) ds = \frac{1}{T} \int_0^T f(s) ds. \tag{14}$$

From Eq. (2) and considering $T = 365$ days as time-windows, we get

$$\langle\alpha\rangle = \frac{1}{365}\int_0^{365}\left[\kappa_1 \sin\left(\frac{2\pi}{365}(t+\omega)\right) + \kappa_2\right]dt, \tag{15}$$

consequently, $\langle\alpha\rangle = \kappa_2$. Then, for t large enough, Eq. (13) admits the approximation:

$$i(t) \approx i(0)\exp\left(\langle\alpha\rangle\frac{\nu}{\rho} - (\rho+\chi)\right)t. \tag{16}$$

Finally, the population of infected birds exhibits growth or decline if and only if

$$\langle\alpha\rangle\frac{\nu}{\rho} - (\rho+\chi) > 0 \quad \Longrightarrow \quad \frac{\nu\langle\alpha\rangle}{\rho(\rho+\chi)} > 1,$$

which brings out the following

$$\mathcal{R}_0 \equiv \frac{\nu\langle\alpha\rangle}{\rho(\rho+\chi)} = \frac{\nu\kappa_2}{\rho(\rho+\chi)}. \tag{17}$$

Therefore, if $\mathcal{R}_0 < 1$, take the limit $\lim_{t\to\infty} i(t) = 0$. On the other hand, if $\mathcal{R}_0 > 1$, then $\lim_{t\to\infty} i(t) \to \infty$.

2.2 Complex dynamics in the model

Equations (1) with a seasonal forcing described by Eq. (2) admit chaotic solutions for a certain range of parameters, as primarily observed in Ref. [13]. By choosing the disease-induced mortality parameter (χ) as a control parameter, we reproduce the result of the bifurcation diagram from [13] in Fig. 2a, where we observe chaotic attractors over a range of parameter values. The magenta dotted line indicates the zero level. The bifurcation diagram in Fig. 2a is calculated by collecting the local maxima of I_b after 190 years of transient. Throughout this work, numerical solutions are obtained through the fourth-order Runge–Kutta method (RK4) [41] with a constant step size equal to 10^{-3}. To determine a correct transient time, we computed the Lyapunov exponents and bifurcation diagrams for several initial conditions using different transient lengths. The transient time was chosen as the minimum integration time for which all the initial conditions considered converged to the corresponding attractor. In this work, we adopted a transient of 190 years. It is important to emphasize that long transient regimes are commonly observed in seasonal epidemiological models [21, 22], in particular in regions close to critical transitions [28].

The bifurcation diagram is obtained by varying the control parameter χ, whose inverse corresponds to the average infectious lifetime of infected birds, over the range corresponding to infectious lifetimes from 2.7 to 3.5 days. Additionally, several periodic ranges are observed in Fig. 2a and b, where the latter displays the largest Lyapunov exponent associated (λ). In this work, the Lyapunov exponents are computed using the Wolf algorithm [42]. The set of parameters used to compute these results is detailed in the caption and is based on Ref. [13]. Although the bifurcation diagram and Lyapunov exponent confirm the existence of chaos, these tools alone do

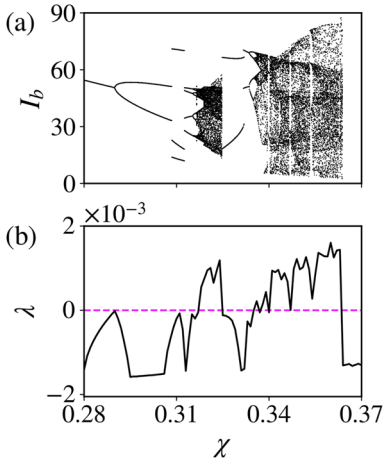


Fig. 2 **a** Bifurcation diagram and **b** the largest Lyapunov exponent as functions of the control parameter χ. The remaining model parameters are $\nu = 1020.0/365.0$, $\rho = 1.0/(2.0 \cdot 365)$, $\kappa_1 = 0.00005111486$, $\kappa_2 = 0.0003262175$, $\omega = 107.75$, $\lambda = 1000/365$, $\beta = 1.9 \times 10^{-11}$ and $\mu = 1/(65 \cdot 365)$

not reveal the coexistence of multiple attractors. To address this question, we next investigate the presence of multistability through hysteresis-type bifurcation diagrams.

3 Multistability

Taking χ as the control parameter, we compute the hysteresis-type bifurcation diagram (HTBD), whose results are shown in Fig. 3(a). To construct it, we consider χ as the control parameter in the interval $\chi \in [\chi_0, \chi_M] \equiv [0.15, 0.64]$, discretized with step size $d\chi = (\chi_M - \chi_0)/M$, where $M = 1000$. Thus, the parameter set is given by $\chi_0, \chi_1, \chi_2, \ldots, \chi_M$.

For the forward direction (red branch in Fig. 3a), the system is initialized at χ_0 with $\mathbf{x}_0 \equiv (S_b(0), I_b(0), S_h(0), I_h(0))$. After discarding a transient of 190 years, the local maxima of I_b are recorded during the subsequent 30 years, producing a final state $\tilde{\mathbf{x}}$. This final state is then used as the initial condition for the next parameter value, e.g. $\chi_1 = \chi_0 + d\chi$. Repeating this procedure up to χ_M produces the forward branch.

To obtain the backward branch (blue points), the same procedure is applied in the reverse direction, starting from χ_M and decreasing the parameter as $\chi_{M-1} = \chi_M - d\chi$. A mismatch between the forward and backward branches indicates hysteresis and the coexistence of attractors [43], and is highlighted by purple and cyan backgrounds in Fig. 3a.

In particular, there are twelve bistable ranges, where two show the coexistence between periodic attractors (purple, region 1), and the remaining display the coexistence between chaotic and periodic attractors (cyan, region 2). Region 2 has increasingly smaller ranges as χ increases and encompasses 9% of the investigated χ range, while region 1 covers 2% of the χ range. Then, the range is dominated by chaotic behavior, and the bistability occurs in 11% of the total parameter range.

Figure 3b displays λ with the corresponding bifurcation shown in Fig. 3a. In the considered range, the model exhibits a rich variety of dynamical regimes, even presenting sudden changes in λ in the regions where the coexistence between chaotic-periodic attractors ends, suggesting the existence of crises [44], which are investigated in the next section. The Lyapunov exponents are consistent with the coexistence of attractors revealed by the HTBDs. Taking into account the values of λ for each branch, we determine the basins of attraction for certain selected regions (Fig. 5).

To clarify the interpretability of the behavior of the attractors, we selected three values of χ, namely $\chi = 0.194$, 0.36 and 0.52, and projected the respective attractors in the plane $S_b \times \log I(b)$, as shown in Fig. 4a–c, respectively. For $\chi = 0.194$, Fig. 4a shows the coexistence of two periodic attractors, as observed in Fig. 3a. These attractors show periodic oscillations of infected and susceptible bird populations, whose oscillations persist with the same amplitude every year, as observed in the respective time series in Fig. 4d.

Furthermore, Fig. 4b presents a projection of two coexistent attractors, but one initial condition leads to periodic dynamics (blue branch), while the red branch leads to chaotic. The period branch leads to periodic oscillation throughout the years, whereas the chaotic time series (Fig. 4e) display discrepancy in maxima of I_b throughout time. In the second time series, the peaks do not repeat themselves in every outbreak, but are irregular.

The last attractor (Fig. 4c), in black, is in a region where only one chaotic attractor exists. For this parametric configuration, the chaotic attractor reaches lower values of I_b than in the previous case, however, the epidemic oscillation is sustained by irregular oscillation, peaking every year.

Next, we explore the basin of attraction in the $S_b(0) \times I_b(0)$ plane of three regions of bistability. Based on $\chi = 0.32$, 0.36 and 0.4448 we compute their basins of attraction composed of a 1000×1000 grid of initial conditions, as exhibited in Fig. 5a–c, respectively. Since our system is multidimensional, we build the attraction basin for the pairs $(S_b(0), I_b(0))$, and the remaining initial conditions are fixed. The grid is discretized into 1000×1000 points. Since there is bistability for the selected χ values, the basins are distinguished by the following color code: initial

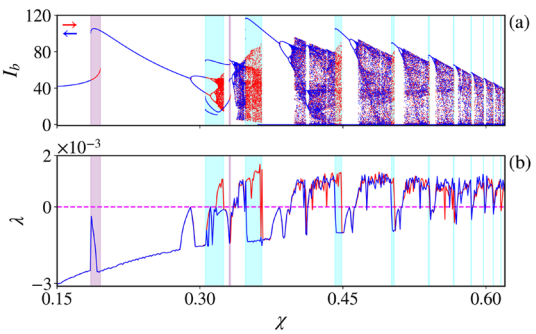


Fig. 3 **a** Hysteresis-type bifurcation diagram of I_b as a function of the control parameter χ and **b** the corresponding largest Lyapunov exponent (λ). Red (blue) denotes forward (backward) continuation of the control parameter

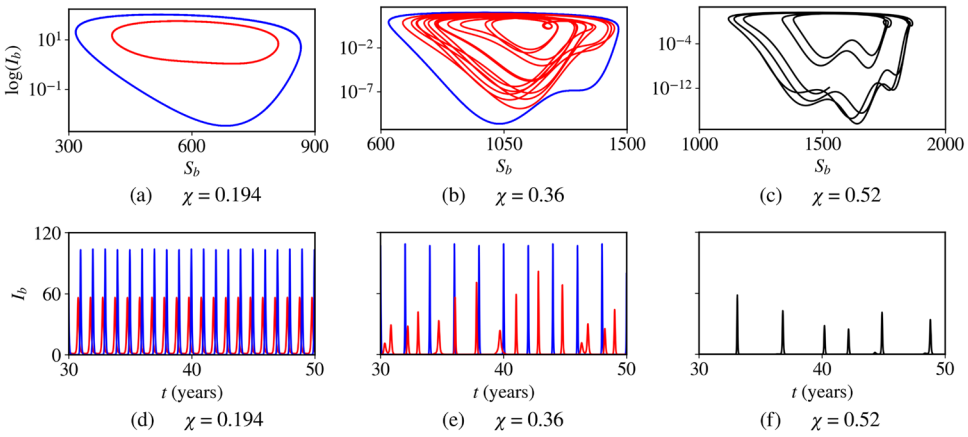


Fig. 4 Projections of the attractors onto the $S_b \times I_b$ plane for $\chi = 0.194$, 0.36, and 0.52 in panels **a**–**c**, respectively. The corresponding time series of I_b associated with each attractor are shown in panels **d**–f, respectively

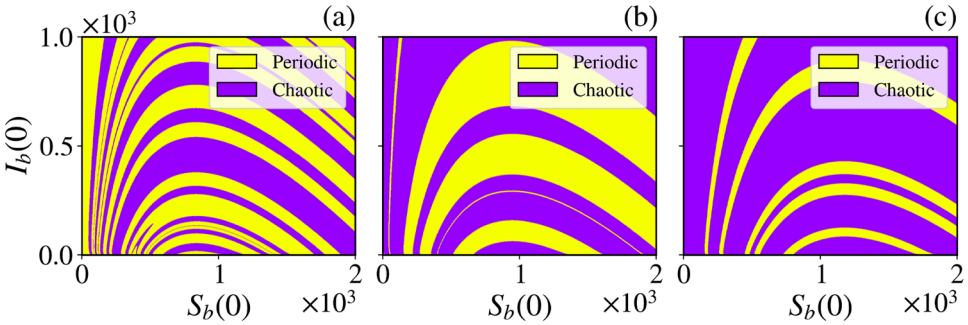


Fig. 5 Basins of attraction in the $S_b(0) \times I_b(0)$ plane for **a** $\chi = 0.32$ (region 2), **b** $\chi = 0.36$ (region 4), and **c** $\chi = 0.4448$. Yellow and purple denote initial conditions converging to the periodic and chaotic attractors

Table 1 Percentage of the basin area associated with the periodic and chaotic attractors shown in Fig. 6

χ	0.32	0.36	0.4448
Periodic (%)	45	51	22
Chaotic (%)	55	49	78

conditions that evolve to a periodic attractor are in yellow, whereas chaotic ones are marked by purple color. Table 1 shows the percentage of the area occupied by each attraction basin for $\chi = 0.32$, the chaotic region is predominant, covering 55% of the total region. For $\chi = 0.36$, the chaotic regions and the periodic ones are almost perfectly split, 51% for the chaotic region and 49% for the periodic one. Finally, for $\chi = 0.4448$, there is a very clear distinction: the chaotic portion occupies 78% of the total region and the periodic portion only 22%. Thus, among the three representative parameter values considered, chaos does not prevail only for $\chi = 0.36$ (among the chosen values). For the remaining two values of χ, the relative basin areas associated with the two attractors are approximately equal, indicating a strong dependence of the long-term dynamics on the initial conditions.

An important feature observed in Fig. 3b is the abrupt disappearance of positive Lyapunov exponents at the edge of some bistable regions. These sudden transitions are often associated with a crisis. This observation motivates a more detailed analysis in the vicinity of the critical parameter, which will be carried out in the next section.

4 Average transient lifetime and crisis

In the vicinity of the critical parameter, the chaotic attractor disappears, leading to a transient chaotic regime. We now explore these transient regimes near the critical points χ_c where λ shows a sudden change, as previously discussed in Fig. 3b.

As the lifetime of a chaotic attractor depends on the initial conditions [45], we consider 1000 randomly chosen initial conditions belonging to the chaotic basin. For each initial condition, we vary χ for $\chi > \chi_c$. For each value of $\chi - \chi_c$, we compute the time when the orbit becomes periodic. Numerically, we identify the critical parameter as $\chi_c = 0.363944$. The transient time and final time chosen here are approximately 110 and 3000 years, respectively. Then, we average all the initial conditions and get $\langle \tau \rangle$, as shown in Fig. 6a by the black points. The red line

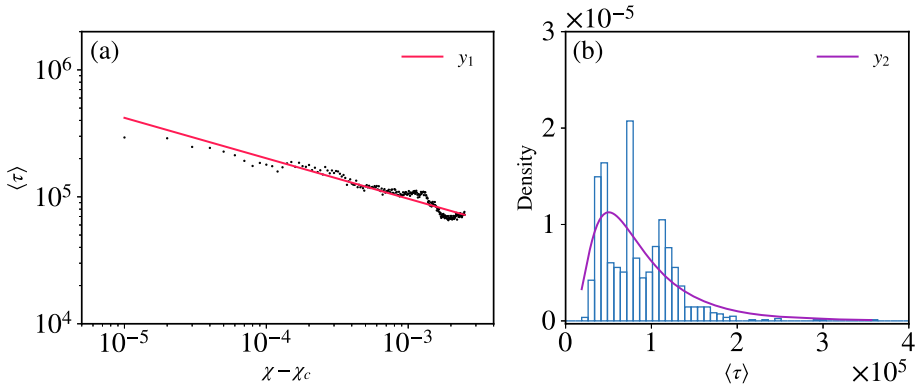


Fig. 6 **a** Average transient lifetime $\langle\tau\rangle$ versus $\chi_c - \chi$ in log-scale for 10^3 different initial conditions. **b** Distribution of the average transient lifetimes. The bars represent the histogram obtained from the data in (a), while the purple curve corresponds to the fitted function y_2

denotes the fitted curve. In Fig. 6b, we show the distribution of transient lifetimes obtained from the sampled initial conditions. The purple curve corresponds to the fit given by

$$f(\langle\tau\rangle) = \frac{A}{\langle\tau\rangle\sigma\sqrt{2\pi}} e^{\frac{(\ln\langle\tau\rangle-\mu)^2}{2\sigma^2}}, \tag{18}$$

where μ, σ, A are the parameters for the fitting. The resulting fit exhibits a maximum at $\langle\tau\rangle$, corresponding to the most probable mean transient time observed in the distribution. In the region under investigation, where transient chaos occurs, the basin of attraction consists of both chaotic and periodic orbits. Nevertheless, the portion of initial conditions that evolves towards the chaotic attractor gradually diminishes as the transient time grows [28]. This solution can be adjusted by a power-law, as observed in Fig. 6b.

It has been theoretically established [44, 46] that the average transient lifetime follows $\langle\tau\rangle \sim |\chi - \chi_c|^{-\gamma}$, where $\gamma > 0$, is the algebraic scaling exponent [47] and is also called the order of crisis. In our study, within the investigated interval of $\chi - \chi_c$, the characteristic exponent is $\gamma = 0.319 \pm 0.007$, with $\chi > \chi_c$, and a correlation coefficient of $R^2(\log - \log) = 0.951707$. This indicates that the data are very well described by a power law. The power-law scaling of $\langle\tau\rangle$, together with the sharp decrease in λ shown in Fig. 3b near χ_c, provides numerical evidence that the observed transition is consistent with a boundary crisis. A crisis is characterized by a collision between a chaotic attractor and an unstable fixed point or a periodic orbit [44]. There are several types of crisis, among them, boundary, interior, fusion, etc. A boundary crisis occurs when a chaotic attractor collides with an unstable periodic orbit that lies on the boundary of its basin of attraction [45, 48]. In general, boundary crises are typically accompanied by transient chaos. After the crisis, the chaotic attractor is immediately destroyed and becomes transient chaos. This happens in our system at the critical parameter χ_c. For example, we construct a basin for $\chi < \chi_c$, such that $\chi = 0.3639$, as exhibited in Fig. 7. The chaotic attractor (black) is observed to collide with the boundary of the basin of attraction of the periodic attractor (red), as $\chi \to \chi_c$. Observing the time, one notices that the chaotic attractor suddenly disappears and is destroyed. However, by analyzing the transient dynamics, we observe a chaotic transient associated with the remnant (or "ghost") of the former chaotic attractor. Trajectories spend many iterations in the remnant before escaping and eventually converging to the periodic attractor [49]. This phenomenon occurs in the Ikeda map following a boundary crisis: the attractor remains an extended time in the "ghost" and then escapes and converges into a fixed point.

In continuous systems (flows), the scaling exponent associated with the average transient lifetime is usually larger than those reported for the logistic and Hénon maps, where $0 < \gamma < 1$ [44]. For the Lorenz system, for example, the crisis order is 4.0 [50]. In high-dimensional systems, the superpersistent regime is frequently observed, in which $\langle\tau\rangle \to \infty$ [47, 51]. In contrast, our system yields $\gamma = 0.319$ as the algebraic scaling exponent, indicating that it exhibits a low-order crisis.

The previous results revealed that the model undergoes crisis-induced transitions capable of destroying chaotic attractors, leading to long transient chaos in the vicinity of the critical parameter. However, for other values of the parameter control, we find regions where trajectories diverge along more than one independent direction in phase space, giving rise to hyperchaotic regimes.

5 Hyperchaos

In chaotic systems, due to the sensitivity to initial conditions, the largest Lyapunov exponent (LE) is positive, followed by a zero exponent, while the remaining ones are necessarily negative [48]. By contrast, a dynamical system

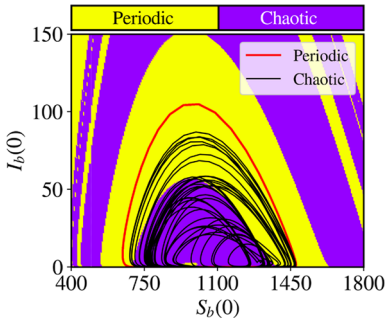


Fig. 7 Basin of attraction before the boundary crisis. Yellow (purple) indicates initial conditions converging to the periodic (chaotic) attractor. The chaotic and periodic attractors are shown in black and red, respectively

Table 2 Type of attractor of the system (1) given by Eqs. (1) based on Lyapunov exponents. Adapted from [53]

Lyapunov exponents	Type of attractor
$\lambda_1 < 0,\ \lambda_2 < 0,\ \lambda_3 < 0,\ \lambda_4 < 0,\ \lambda_5 = 0$	Periodic attractor
$\lambda_1 > 0,\ \lambda_2 < 0,\ \lambda_3 < 0,\ \lambda_4 < 0,\ \lambda_5 = 0$	Chaotic attractor
$\lambda_1 > 0,\ \lambda_2 > 0,\ \lambda_3 < 0,\ \lambda_4 < 0,\ \lambda_5 = 0$	Hyperchaotic attractor

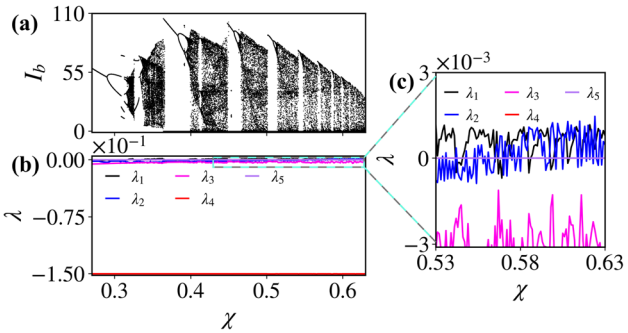


Fig. 8 **a** Bifurcation diagram for I_b as a function of χ. **b** Lyapunov exponents λ_i, $i = 1, ..., 5$ as functions of χ. In **c**, a blow-up of panel (b)

that exhibits hyperchaos presents two or more positive Lyapunov exponents [52]. To the best of our knowledge, hyperchaos in epidemic models was first registered by Yi et al. [53] in 2009 in an SEIR model with seasonality. They reported that hyperchaos is present only for certain values of parameters. Additionally, in a more complex scenario, Aguiar et al. [22] reported hyperchaotic solutions for a seasonal multi-strain dengue epidemic model.

In our system, we find that adjusting the control parameter χ upward leads to periodic windows and chaotic regimes, as evidenced by λ, as shown in Figs. 2 and 3. Table 2 presents the types of attractor associated with the LE values for the avian flu model. In Fig. 8b, we compute the Lyapunov spectrum λ_i ($i = 1, 2, 3, 4, 5$), which satisfies condition $\lambda_1 \geq \lambda_2 \geq \lambda_3 \geq \lambda_4 \geq \lambda_5$. The exponent associated with the forcing is always null. For λ_1 and λ_2, they alternate between periodic and chaotic behavior for $\chi > 0.50$, the system exhibits λ_1, $\lambda_2 > 0$, as shown in Fig. 8c. The small positive Lyapunov exponents obtained in our system (of the order of 10^{-3}) can indicate that its dynamics may be governed by weak chaos [54]. In general, we note that systems with large dimensionality exhibit Lyapunov exponents of small magnitude. For instance, in their model of two coupled neuronal populations, Olmi et al. [55] demonstrated that the largest Lyapunov exponent is positive and has a magnitude on the order of 10^{-2}. Thottil et al. [56] explored several coupled Hindmarsh-Rose models, showing that the positive Lyapunov exponents also have a low magnitude, close to zero.

6 Conclusions

In this work, we extend the study of a mathematical model for avian influenza proposed by Tuncer and Martcheva [13]. We identify bistability, transient chaos, crisis, and hyperchaos.

When constructing the hysteresis-type bifurcation diagram, a bistable regime becomes evident. Among the twelve bistable regions identified, ten correspond to the coexistence of periodic and chaotic attractors, while two regions exhibit the coexistence of two distinct periodic solutions. To obtain this diagram, the final state of each simulation is used as the initial condition for the subsequent parameter value, which allows the system to follow different solution branches.

For certain values of the control parameter, the chaotic attractor is abruptly destroyed in a boundary crisis. In the vicinity of this critical parameter, the system exhibits a transient chaos with a lifetime distribution for an ensemble of initial conditions. On the other hand, for this ensemble, the mean transient lifetime can be described by a power-law scaling $(\chi - \chi_c)^{-\gamma}$ with $\gamma = 0.319 \pm 0.007$, in agreement with crisis-induced dynamics.

Moreover, the occurrence of hyperchaos, evidenced by multiple positive Lyapunov exponents, reveals high-dimensional instability and increased dynamical complexity. In the epidemiological context, hyperchaotic regimes are less studied, with a few examples including the work of Yi [53] and Aguiar et al. [22]. Therefore, we show that, beyond the classical chaotic routes and the new bistable solutions, the system also admits hyperchaotic regimes.

Our analysis reveals that the model exhibits bistability, boundary crises, transient chaos, and hyperchaotic regimes, non-linear phenomena that had not previously been reported for this model. Together, these results provide a more comprehensive characterization of the non-linear dynamics exhibited by this seasonally forced epidemiological model. We hope that this study contributes to a better understanding of the non-linear dynamics of seasonally forced epidemiological models and provides new insights into the complex transmission dynamics of avian influenza.

Acknowledgements The authors thank the financial support from the Brazilian Federal Agencies (CNPq), under grant 302665/2017-0; CAPES; Fundação Araucária. São Paulo Research Foundation (FAPESP) under grants 2025/05453-0, 2024/13613-5, 2024/05700-5, 2025/02318-5, 2025/14690-6, and 2025/24097-0. J.K. was supported by Research start-up funds for introducing talents of the Fudan University (IDH2315001 Y). We would like to thank www.105groupscience.com and Professor Ulrike Feudel for valuable discussions.

Funding The Article Processing Charge (APC) for the publication of this research was funded by the Coordenação de Aperfeiçoamento de Pessoal de Nível Superior - Brasil (CAPES) (ROR identifier: 00x0ma614).

Data Availability Data supporting the findings of this study are available upon reasonable request.

Open Access This article is licensed under a Creative Commons Attribution 4.0 International License, which permits use, sharing, adaptation, distribution and reproduction in any medium or format, as long as you give appropriate credit to the original author(s) and the source, provide a link to the Creative Commons licence, and indicate if changes were made. The images or other third party material in this article are included in the article's Creative Commons licence, unless indicated otherwise in a credit line to the material. If material is not included in the article's Creative Commons licence and your intended use is not permitted by statutory regulation or exceeds the permitted use, you will need to obtain permission directly from the copyright holder. To view a copy of this licence, visit http://creativecommons.org/licenses/by/4.0/.

References

1. P. Palese, J.F. Young, Variation of influenza a, b, and c viruses. Science **215**(4539), 1468–1474 (1982)
2. W. Schäfer, Vergleichende sero-immunologische untersuchungen über die viren der influenza und klassischen geflügelpest. Zeitschrift für Naturforschung B **10**(2), 81–91 (1955)
3. D.J. Alexander. An overview of the epidemiology of avian influenza. *Vaccine*, 25(30):5637–5644, 2007. 4th International Veterinary Vaccines and Diagnostics Conference, Oslo, 25-29 June (2006)
4. H.G. Pereira, B. Tumová, V.G. Law, Avian influenza a viruses. Bull. World Health Organ. **32**, 855–860 (1965)
5. World Health Organization. H5N1 highly pathogenic avian influenza: Timeline of major events. WHO, 2014
6. S. Iwami, Y. Takeuchi, X. Liu, Avian-human influenza epidemic model. Math. Biosci. **207**, 1–25 (2007)
7. C.R. Andrade, C.C. Ibiapina, N.S. Champs, A.C.C. Toledo Jr., I.F.M. Picinin, Gripe aviária: a ameaça do século XXI. J. Bras. Pneumol. **35**(5), 470–479 (2009)
8. G. Morel, A. Pham, C. Morgenstern, J.T. Hicks, T. Rawson, V.Y. Fan, W.J. Edmunds, G. Forchini, K. Hauck, An outbreak of highly pathogenic avian influenza h5n1 could impact the dairy cattle sector and the broader economy in the united states. Communications Earth & Environment **7**(1), 135 (2026)
9. P.M. Neufeld. Memória médica: a gripe espanhola de 1918. *Revista Brasileira de Análises Clínicas*, pages 213–217, (2020)
10. M.R. Donalísio, Influenza aviária: questões centrais. Revista Brasileira de Pneumologia **1**(9), 7–19 (2005)
11. I.N. Kandun, G. Samaan, S. Harun, W.H. Purba, E. Sariwati, E. Septiawati, M. Silitonga, N.P. Dharmayanti, P.M. Kelly, T. Wandra, Chicken faeces garden fertilizer: possible source of human avian influenza h5n1 infection. Zoonoses Public Health **57**(4), 285–290 (2010)
12. S.L.T. de Souza, A.M. Batista, I.L. Caldas, K.C. Iarosz, J.D. Szezech Jr., Dynamics of epidemics: Impact of easing restrictions and control of infection spread. Chaos, Solitons Fractals **142**, 110431 (2021)
13. N. Tuncer and M. Martcheva. Modeling seasonality in avian influenza H5N1. Journal of Biological Systems, 21:1340004–1–1340004–30, (2013)
14. M. Martcheva, An evolutionary model of influenza a with drift and shift. J. Biol. Dyn. **6**, 299–332 (2012)

15. A.W. Park, K. Glass, Dynamic patterns of avian and human influenza in east and southeast asia. Lancet. Infect. Dis **7**(5), 543–548 (2007)
16. K.S. Li, Y. Guan, J. Wang, G.J.D. Smith, K.M. Xu, L. Duan, A.P. Rahardjo, P. Puthavathana, C. Buranathai, T.D. Nguyen, A.T.S. Estoepangestie, A. Chaisingh, P. Auewarakul, H.T. Long, N.T.H. Hanh, R.J. Webby, L.L.M. Poon, H. Chen, K.F. Shortridge, K.Y. Yuen, R.G. Webster, J.S.M. Peiris, Genesis of a highly pathogenic and potentially pandemic h5n1 influenza virus in eastern asia. Nature **430**(6996), 209–213 (2004)
17. E.J. Murray, S.S. Morse, Oscillation of human infection with influenza a/h5n1 in egypt and indonesia. PLoS ONE **6**, e24042 (2011)
18. F.E. Cruziniani, E.C. Gabrick, A.L.R. Moraes, M.S. Santos, A.M. Batista, J. Trobia, K.C. Iarosz, I.L. Caldas, and J. Kurths. Epidemic model with seasonality for avian influenza waves in humans. The European Physical Journal Special Topics, pages 1–16, (2026)
19. S. Altizer, A. Dobson, P. Hosseini, P. Hudson, M. Pascual, P. Rohani, Seasonality and the dynamics of infectious diseases. Ecol. Lett. **9**, 467–484 (2006)
20. L.F. Olsen, W.M. Schaffer, Chaos versus noisy periodicity: alternative hypotheses for childhood epidemics. Science **249**, 499–504 (1990)
21. B.D. Dalziel, O.N. Bjornstad, W.G. van Panhuis, D.S. Burke, C.J.E. Metcalf, and B.T. Grenfell. Persistent chaos of measles epidemics in the prevaccination united states caused by a small change in seasonal transmission patterns. PLOS Computational Biology, 12(2):1–12, 02 (2016)
22. M. Aguiar, S. Ballesteros, B.W. Kooi, N. Stollenwerk, The role of seasonality and import in a minimalistic multi-strain dengue model capturing differences between primary and secondary infections: Complex dynamics and its implications for data analysis. J. Theor. Biol. **289**, 181–196 (2011)
23. M. Aguiar, B. Kooi, N. Stollenwerk, Epidemiology of dengue fever: A model with temporary cross-immunity and possible secondary infection shows bifurcations and chaotic behaviour in wide parameter regions. Math. Model. Nat. Phenom. **3**, 48–70 (2008)
24. M. Aguiar, N. Stollenwerk, B.W. Kooi, Torus bifurcations, isolas and chaotic attractors in a simple dengue fever model with ade and temporary cross immunity. Int. J. Comput. Math. **86**(10–11), 1867–1877 (2009)
25. J.L. Aron, I.B. Schwartz, Seasonality and period-doubling bifurcations in an epidemic model. J. Theor. Biol. **110**, 665–679 (1984)
26. N. Stollenwerk, S. Spaziani, J. Mar, I.E. Arrizabalaga, D. Knopoff, N. Cusimano, V. Anam, A. Shrivastava, M. Aguiar, Seasonally Forced SIR Systems Applied to Respiratory Infectious Diseases, Bifurcations, and Chaos. Computational and Mathematical Methods **2022**(1), 3556043 (2022)
27. B.T. Grenfell, B.M. Bolker, A. Kleczkowski, Seasonality and extinction in chaotic metapopulations. Proc. R. Soc. Lond. B **259**, 97–103 (1995)
28. E.C. Gabrick, E. Sayari, P.R. Protachevicz, J.D. Szezech Jr., K.C. Iarosz, S.L.T. de Souza, A.C.L. Almeida, R.L. Viana, I.L. Caldas, A.M. Batista, Unpredictability in seasonal infectious diseases spread. Chaos, Solitons Fractals **166**, 113001 (2023)
29. W.P. London, J.A. Yorke, Recurrent outbreaks of measles, chickenpox and mumps: I. seasonal variation in contact rates. Am. J. Epidemiol. **98**, 453–468 (1973)
30. M. Aguiar, V. Anam, K.B. Blyuss, C.D.S. Estadilla, B.V. Guerrero, D. Knopoff, B.W. Kooi, A.K. Srivastav, V. Steindorf, N. Stollenwerk, Mathematical models for dengue fever epidemiology: A 10-year systematic review. Phys. Life Rev. **40**, 65–92 (2022)
31. D.J.D. Earn, P. Rohani, B.M. Bolker, B.T. Grenfell, A simple model for complex dynamical transitions in epidemics. Science **287**, 667–670 (2000)
32. M.J. Keeling, P. Rohani, B.T. Grenfell, Seasonally forced disease dynamics explored as switching between attractors. Physica D **148**, 317–335 (2001)
33. E.C. Gabrick, E.L. Brugnago, A.L.R. de Moraes, P.R. Protachevicz, S.T. da Silva, F.S. Borges, I.L. Caldas, A.M. Batista, and Jürgen Kurths. Control, bi-stability, and preference for chaos in time-dependent vaccination campaign. Chaos: An Interdisciplinary Journal of Nonlinear Science, 34(9):093118, (2024)
34. B.T. Grenfell, A. Kleczkowski, C.A. Gilligan, B.M. Bolker, Spatial heterogeneity, nonlinear dynamics and chaos in infectious diseases. Stat. Methods Med. Res. 4, (1995)
35. D.J.D. Earn, P. Rohani, B.T. Grenfell, Persistence, chaos and synchrony in ecology and epidemiology. Proc. R. Soc. Lond. B **265**, 7–10 (1998)
36. M.J. Keeling, P. Rohani, *Modeling Infectious Diseases in Humans and Animals*, 1st edn. (Princeton University Press, Princeton, 2008)
37. S. Bilal, B.K. Singh, A. Prasad, E. Michael, Effects of quasiperiodic forcing in epidemic models. Chaos **26**, 093115 (2016)
38. E.L. Brugnago, E.C. Gabrick, K.C. Iarosz, J.D. Szezech Jr., R.L. Viana, A.M. Batista, I.L. Caldas, Multistability and chaos in seirs epidemic model with a periodic time-dependent transmission rate. Chaos **33**, 123123 (2023)
39. M. Martcheva, *An Introduction to Mathematical Epidemiology,* vol. 61, 1st edn. (Springer, New York, 2015)
40. J. Ma, Z. Ma, Epidemic threshold conditions for seasonally forced seir models. Math. Biosci. Eng. **3**, 161–172 (2006)
41. W.E. Boyce, R.C. DiPrima, *Elementary Differential Equations and Boundary Value Problems*, 10th edn. (John Wiley and Sons Ltd, New Jersey, 2012)

42. A. Wolf, J.B. Swift, H.L. Swinney, J.A. Vastano, Determining lyapunov exponents from a time series. Physica D **16**, 285–317 (1985)
43. E.S. Medeiros, I.L. Caldas, M.S. Baptista, U. Feudel, Trapping phenomenon attenuates the consequences of tipping points for limit cycles. Sci. Rep. **7**(1), 42351 (2017)
44. C. Grebogi, E. Ott, J.A. Yorke, Crises, sudden changes in chaotic attractors, and transient chaos. Physica D **7**(1), 181–200 (1983)
45. Y.-C. Lai, T. Tél, *Transient Chaos*, 1st edn. (Springer, New York, NY, New York, 2011)
46. C. Grebogi, E. Ott, F. Romeiras, J.A. Yorke, Critical exponents for crisis-induced intermittency. Phys. Rev. A **36**, 5365–5380 (1987)
47. V. Andrade, Y.-C. Lai, Super persistent chaotic transients in physical systems: Effect of noise on phase synchronization of coupled chaotic oscillators. International Journal of Bifurcation and Chaos **11**(10), 2607–2619 (2001)
48. R.L. Viana, Introdução à dinâmica não-linear e caos (Paraná, Brasil, 1, 2023), (Departamento de Física)
49. K.T. Alligood, T.D. Sauer, J.A. Yorke, *CHAOS: An Introduction to Dynamical Systems,* vol. 1, 1st edn. (Springer, New York, 1996)
50. J.A. Yorke, E.D. Yorke, Metastable chaos: The transition to sustained chaotic behavior in the Lorenz model. J. Stat. Phys. **21**(3), 263–277 (1979)
51. C. Grebogi, E. Ott, J.A. Yorke, Super persistent chaotic transients. Ergodic Theory Dynam. Systems **5**(3), 341–372 (1985)
52. S.L. Kingston, T. Kapitaniak, and S.K. Dana. Transition to hyperchaos: Sudden expansion of attractor and intermittent large-amplitude events in dynamical systems. *Chaos: An Interdisciplinary Journal of Nonlinear Science*, 32(8):081106, 08 (2022)
53. N. Yi, Q. Zhang, K. Mao, D. Yang, Q. Li, Analysis and control of an SEIR epidemic system with nonlinear transmission rate. Math. Comput. Model. **50**, 1498–1513 (2009)
54. C.P. Gonçalves and C. Rouco. Stochastic chaos in influenza data - an application of topological methods. medRxiv, pages 1–45, (2025)
55. S. Olmi, A. Politi, A. Torcini, Collective chaos in pulse-coupled neural networks. Europhys. Lett. **92**(6), 60007 (2011)
56. S.K. Thottil, R.P. Ignatius, Nonlinear feedback coupling in Hindmarsh-Rose neurons. Nonlinear Dyn. **87**(3), 1879–1899 (2017)